Magnetic ionic liquid/polymer composites: tailoring physico-chemical properties by ionic liquid content and solvent evaporation temperature

Daniela M. Correia[1,2,*+], Liliana Fernandes[2,+], Clara García-Astrain[2], Mohammad Tariq[3], José M.S.S. Esperança[3], Verónica de Zea Bermudez[1], Senentxu Lanceros Méndez[2, 4*]

[1]Department of Chemistry and CQ-VR, University of Trás-os-Montes e Alto Douro, 5000-801 Vila Real, Portugal

[2]BCMaterials, Basque Center for Materials, Applications and Nanostructures, UPV/EHU Science Park, 48940 Leioa, Spain

[3]LAQV, REQUIMTE, Departamento de Química, Faculdade de Ciências e Tecnologia, Universidade Nova de Lisboa, 2829-516 Caparica, Portugal

[4]IKERBASQUE, Basque Foundation for Science, 48013 Bilbao, Spain

+equal contribution

* Corresponding authors

E-mail: senentxu.lanceros@bcmaterials.net

dcorreia@utad.pt

Abstract

This works reports on the development of magnetic composites based on the magnetic ionic liquid (MIL) 1-butyl-3-methylimidazolium tetrachloroferrate, ([Bmim][$FeCl_4$]) and the electroactive polymer poly(vinylidene fluoride-trifluorethylene) (P(VDF-TrFE)). The composites were obtained at different solvent evaporation temperatures (≈25, 90 and 210 ºC) and with different MIL contents (10, 20 and 40 wt.%). It was concluded that the composites morphology is dependent on the evaporation temperature, allowing to obtain porous membranes with interconnected pores. A decrease in the crystallinity degree resulted upon increasing MIL content. The stability of P(VDF-TrFE) is slightly affected by the inclusion of MIL and by the solvent evaporation temperature used during the processing of the composites. The composites exhibit paramagnetic behavior. Tailoring of the magnetic susceptibility was possible through the control of the MIL content and solvent evaporation temperature.

1.Introduction

Smart materials are materials with the ability to adapt to different surrounding conditions by changing their intrinsic properties upon application of an external stimuli, such as stress, temperature, pH, electromagnetic fields, among others [1]. Electroactive polymers (EAPs) gained special attention due to their attractive advantages, such as lightweight, cost effectiveness, easy processability, flexibility and tolerance to fracture, and additional functionalities. These features allow obtain polymer-based smart materials with tailored active responses to different external stimuli [2]. This versatility of EAPs make those materials very attractive for a wide range of applications, namely for energy storage and generation [3], biomedicine [4], sensor and actuators [5], among others [6]. Compared to other smart material systems, EAPs offer several clear advantages, in particular high response speed (μs to min), low density (1-2 g cm^{-3}), high resilience and high actuation strains (over 300-400%) [7].

Among all EAPs, Nafion, poly(vinylidene fluoride) (PVDF) and PVDF-based copolymers are the most commonly used. PVDF is a semi-crystalline biocompatible polymer with interesting intrinsic properties, such as high electroactive response, dielectric constant, ionic conductivity and polarity [8]. This polymer presents five different phases depending on the chain conformation (α, β and γ), the β phase being the main responsible for its piezoelectric properties [9]. PVDF and its copolymers can be processed in different forms and shapes and applied in several areas, such as tissue engineering, sensors and actuators, among others [3a, 4a, 6d]. Independently of the processing method and for specific molar ratios, the PVDF-poly(vinylidene fluoride-trifluoroethylene) (P(VDF-TrFE) copolymer presents the ferroelectric β crystalline phase, due to the addition of a third fluoride atom in the TrFE monomer unit [8].

EAPs can be divided into two classes: electronic and ionic [6b], with different response times, forces and bending. Electronic EAPs are a more developed technology when compared to ionic EAPs due to their durability under open air atmosphere conditions. To overcome such limitation, the development of systems composed of electronic EAPs and ionic liquids (ILs) are a promising solution [2].

ILs gained special interest due to their tunable physical-chemical properties, such as, high ionic conductivity [10], electrochemical and thermal stability [11], non-flammability [11a], negligible vapor pressure [12], as well as the ability to be used as solvents, representing in many cases a green and clean solution to replace commonly used volatile solvents [13]. Depending on the cation or anion type it is possible to optimize their structure and properties, such as conductivity and electrochemical stability [11b].

Recently, a great interest has been devoted to magnetic ionic liquids (MILs), such as 1-butyl-3-methylimidazolium tetrachloroferrate ([Bmim][$FeCl_4$]) [14]. The major advantage of MILs is associated with their ability to respond to an external magnetic field upon incorporation of magnetic constituents, such as, transition (iron and cobalt)or rare earth metal ions [13a, 15].

Composites based on MILs and EAPs [16] allow the development of an entirely new class of electroactive smart materials combining highly polar matrices with ionic mobile species [17], and exhibiting suitable magnetic, electric, mechanical and electromechanical properties [6d]. Different IL/polymer composites have been developed targeting different fields, such as biomedicine, and sensor and actuator applications [8]. However, to the best of our knowledge, few studies have been reported on the development of composites combining piezoelectric polymers with MILs [18].

In this work, magnetically responsive P(VDF-TrFE)/[Bmim][$FeCl_4$] composites were synthesized by solvent casting. The composites were prepared at different solvent

evaporation temperatures (room temperature, 90 and 210 ^{o}C) and various MIL concentrations (10, 20 and 40 % wt). The morphology, physical-chemical and thermal properties were evaluated. The magnetic properties of all composites were also analyzed.

2. Materials and Methods

2.1. Materials

[Bmim][$FeCl_4$] (99%) (Figure 1a and 1b) was synthesized as reported in [15c]. P(VDF-TrFE) (350000 g.mol^{-1}, Solvay) (Figure 1c) and N,N-dimethylformamide (DMF) (99.5%, Merck) were used as received.

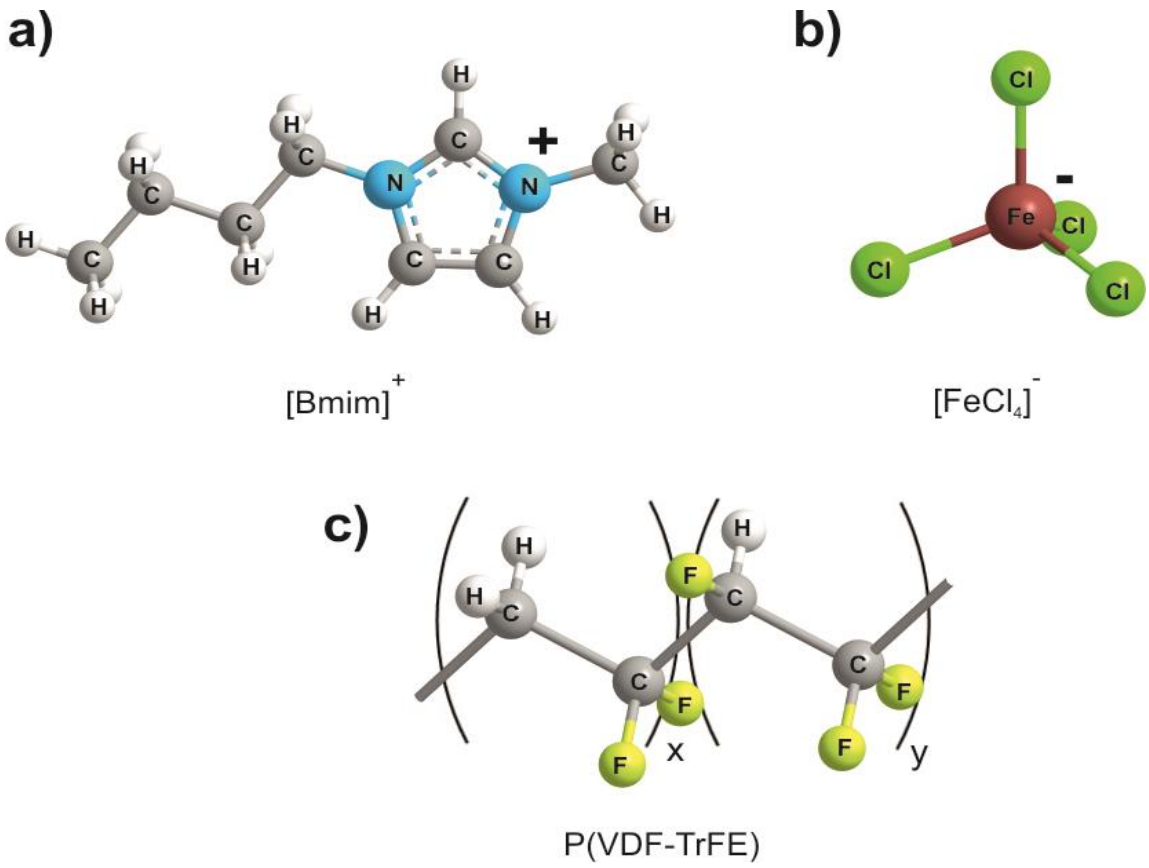

Figure 1. Chemical structures of the MIL cation (a) and anion (b) and of P(VDF-TrFE) (c).

2.2. Preparation of the composite films

P(VDF-TrFE) was dissolved in DMF in a ratio of 15/85 wt.% under mechanical agitation at room temperature. After complete dissolution of the polymer, different contents of the [Bmim][$FeCl_4$] MIL (10, 20 and 40 % (wt.%)) were added to the solution. P(VDF-TrFE)/[Bmim][$FeCl_4$] films with a thickness of ≈50 μm were obtained after spreading the solution at room temperature on a clean glass substrate, followed by solvent evaporation at different temperatures (room temperature, 90 and 210 ºC in an air oven). The study of effect of the solvent evaporation temperature was performed for composites with 40% wt. of MIL.

2.3. Characterization

2.3.1. Morphology

The morphology of the P(VDF-TrFE)/[Bmim][$FeCl_4$] films was analyzed using a scanning electron microscope (SEM, NanoSEM – FEI Nova 200) with an accelerating voltage of 10 kV. The samples were previously coated with a thin gold layer using a sputter coating (Polaron, model SC502).

2.3.2. Physical-chemical characterization

Fourier transformed infrared (FTIR) measurements were performed at room temperature in a Thermo Nicolet Nexus 670 in attenuated total reflectance (ATR) mode from 4000 to 400 cm^{-1}, using 64 scans at a resolution of 4 cm^{-1}.

Differential scanning calorimetry measurements (DSC) were performed in a Perkin-Elmer DSC 8000 apparatus between 30 and 200 °C using a heating rate of 10 $ºC.min^{-1}$ under nitrogen purge. The degree of crystallinity (Xc) of each sample was evaluated using equation 1 [19]:

$$\chi_c = \frac{\Delta H_f}{\Delta H_{100}} \times 100 \quad (1)$$

where ΔH_f is the melting enthalpy of the sample and ΔH_{100} is the melting enthalpy for a 100% crystalline sample (ΔH_{100} = 103.4 J.g^{-1} for P(VDF-TrFE) [19]).

The thermogravimetric analysis (TGA) was performed using a DTG-60 Shimadzu apparatus operating between 40 and 800 °C. A heating rate of 10 °C.min^{-1} and a nitrogen atmosphere were used in all experiments. Samples were placed in α-Al_2O_3 pans.

The magnetic behavior of the MIL and composites were measured at room temperature using a Quantum Design's MPMS 3 superconducting quantum interference device (SQUID) from -20 kOe to 20 kOe.

3. Results and discussion

To evaluate the influence of the solvent evaporation temperature on the morphology of the composites, samples with the highest content of MIL (40 wt.%) were analyzed by SEM (Figure 2).

Figure 2 shows that the preparation of the composites at different evaporation temperatures led to different porous structures with different pore size and degree of porosity. Figure 2a allows observing that when the solvent evaporation occurs at room temperature, the P(VDF-TrFE)/[Bmim][$FeCl_4$] composites present the characteristic porous structure of β-P(VDF-TrFE) crystalline phase originating from the spinodal liquid-liquid phase separation [20] with a porous mean dimeter of 36±7 μm. The presence of the MIL within the polymer matrix and in its walls is also detected. The number of interconnected pores increases, and the size of the pores decreases with an increase in the

solvent evaporation temperature. For a solvent evaporation temperature of 90 ºC a higher number of porous with a mean diameter of 4.2±0.9 µm can be observed. Under these conditions the MIL is entrapped in the polymer matrix and in and out of the pores of the polymer matrix (Figure 2b-c).

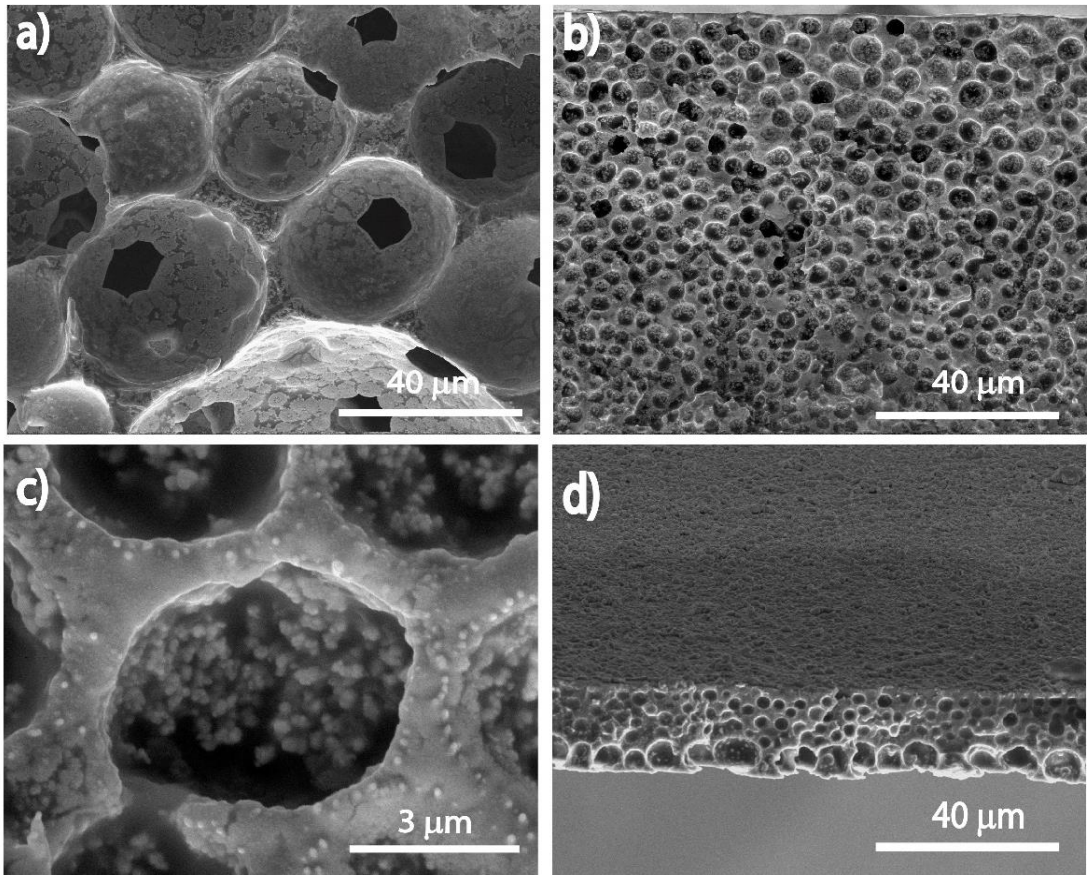

Figure 2. SEM images of the P(VDF-TrFE)/[Bmim][$FeCl_4$] composite films with 40 wt.% of MIL prepared at different solvent evaporation temperature: room temperature (a), 90 ºC (b) and (c), and 210 ºC (d).

The same tendency is observed for the P(VDF-TrFE)/[Bmim][$FeCl_4$] composites obtained at a solvent evaporation temperature of 210 ºC. Generally, at this temperature the P(VDF-TrFE) polymer chains acquire the necessary mobility to occupy the free space left by solvent evaporation, leading to a more compact structure [18, 21]. It is also noticed

that the pore sizes decrease (mean diameter of 2.6±0.6 μm) with increasing solvent evaporation temperature from 90 to 210 ºC. This result indicates that the inclusion of the MIL into the polymer matrix induces the observed porosity, the number of pores being thus associated with the solvent evaporation temperature. When the solvent starts to evaporate, the MIL is encapsulated in the P(VDF-TrFE) polymer structure since it tends to move to the space previously occupied by DMF [18].

A more compact structure is formed when the solvent evaporation increases, because a higher amount of MIL is encapsulated inside to the polymer matrix. This induced us to study in further detail the effect of MIL content in the polymer matrix in composites in which the solvent evaporation occurred at 210 ºC.

The influence of the solvent evaporation temperature and [Bmim][$FeCl_4$] content on the chemical properties of P(VDF-TrFE) was evaluated by ATR-FTIR measurements.

Figure 3 shows the ATR-FTIR spectra of the P(VDF-TrFE)/[Bmim][$FeCl_4$] composites obtained at different solvent evaporation temperatures with an IL content of 40% wt. (Figure 3a) and with different MIL contents (Figure 3b). The bands at 1432 and 1398 cm^{-1} are assigned to the bending and wagging vibrational modes of CH_2, and to the symmetric stretching vibration of C-C group, respectively [22]. The bands at approximately 1171, 882, 842, 502, 465 and 411 cm^{-1} can be assigned to the stretching vibration of the group CF_2. The feature at 842 cm^{-1} is the band assigned to the β-phase of the polymer [22]. No other polymer characteristic phases were observed since, it is known that for solvent evaporation temperatures up to 80 °C, the chain entanglements of the polymer chain lead to an oriented packing of CH_2–CF_2 dipoles promoting the nucleation of the β-phase [23].

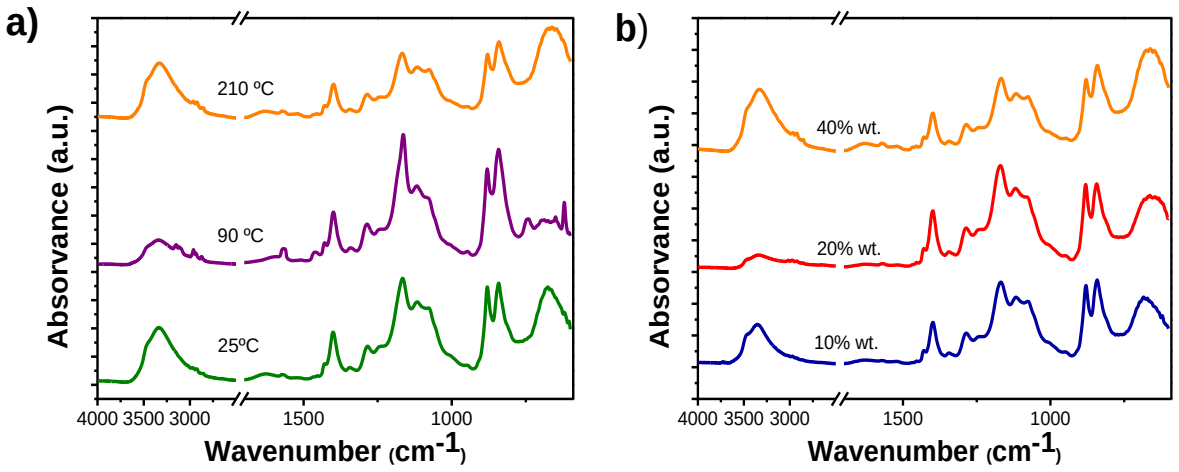

Figure 3. ATR-FTIR spectra for the P(VDF-TrFE)/[Bmim][$FeCl_4$] composites obtained at different solvent evaporation temperatures with 40% wt. of MIL (a) and with different MIL contents at 210 ºC (b).

The ATR-FTIR spectra of Figures 3a and 3b demonstrate that the main characteristics absorption bands of the P(VDF-TrFE) are not suppressed after the incorporation of the MIL. It is also possible to conclude from these spectral data that, independently of the solvent evaporation temperature and IL content, the P(VDF-TrFE)/[Bmim][$FeCl_4$] composites crystallize mainly in the ferroelectric β-phase. This finding is in perfect agreement with the fact that, no matter the processing method, P(VDF-TrFE) crystallizes in the electroactive β-phase for VDF contents ranging from 50 to 80% [8]. The absorption bands observed in the composites at approximately 3150, 3110, 1162, 638, and 613 cm^{-1} are assigned to aromatic C-H vibrations of the $[Bmim]^+$ cations [24]. The bands at 2961, 2932, 1459, 829, and 736 cm^{-1} are assigned to aliphatic C–H vibrations of the $[Bmim]^+$ cations [24]. The C–C and C–N stretching vibrations of $[Bmim]^+$ are found at 1564 cm^{-1} [24]. Figure 3b reveals that, as expected, the intensity of the characteristic absorption bands of [Bmim][$FeCl_4$] increases with the increase of MIL content. Furthermore, it is also possible to detect a decrease in the intensity of absorption bands characteristic of the

P(VDF-TrFE) polymer. These results indicate a very weak chemical interaction between P(VDF-TrFE) and [Bmim][$FeCl_4$], suggesting the occurrence of physical interactions.

3.3. Thermal characterization

The DSC thermograms of the P(VDF-TrFE)/[Bmim][$FeCl_4$] composites obtained at different temperatures and with different MIL contents are shown in Figure 4. As expected, two endothermic peaks are observed in the composites. The lower temperature peak centered around 93 ºC corresponds to the ferroelectric-paraelectric phase transition (Curie temperature, T_C) and the higher temperature peak centered between 120 and 145 ºC corresponds to the melting temperature (T_m) of the polymer [19].

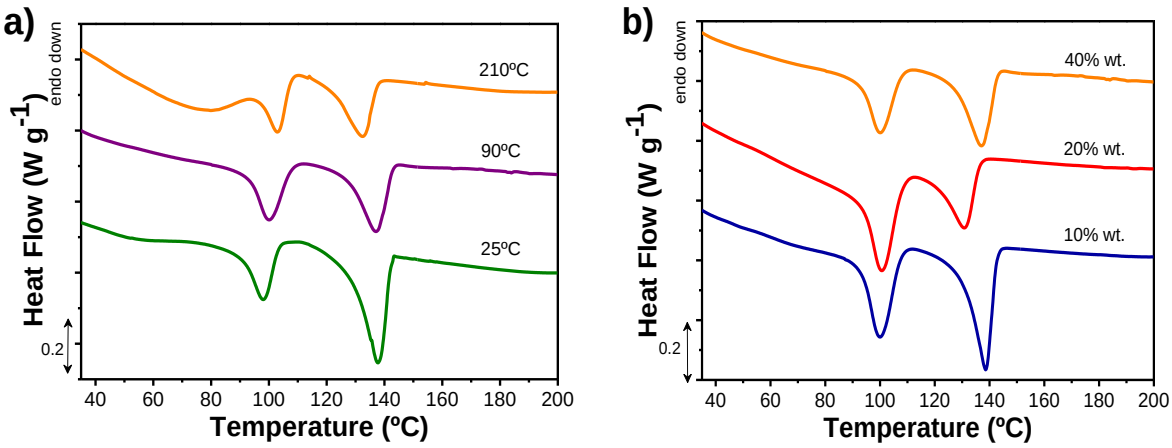

Figure 4. DSC thermograms of the P(VDF-TrFE)/[Bmim][$FeCl_4$] composites obtained at different solvent evaporation temperatures and a MIL content of 40% wt. (a) and with different contents of MIL (b).

As shown in Table 1, the incorporation of [Bmim][$FeCl_4$] into the P(VDF-TrFE) matrix promotes a slight shift of T_C to lower temperatures and a larger decrease in the T_m value with respect to the pure copolymer, being both nearly independent of the IL content. Both shifts are indicative of the miscibility and compatibility between the polymer chains and

the MIL [25] as well as on the destabilization of the ferroelectric and crystalline phases due to the defects introduced by the filler.

The influence of the temperature and MIL content on the X_c value of the P(VDF-TrFE) within the samples was determined from the DSC curves using equation 1 (Table 1).

Table 1. Relevant thermal parameters for pristine P(VDF-TrFE) and for the polymer within the P(VDF-TrFE)/[Bmim][$FeCl_4$] composites.

		T_C (ºC)	**T_m (ºC)**	**$\chi_c \pm 3$ (%)**
P(VDF-TrFE)		105[21]	150[21]	28[26]
P(VDF-TrFE)/[Bmim][$FeCl_4$]				
Solvent evaporation temperature	25 ºC	98	137	16
	90 ºC	103	132	24
	210 ºC	100	137	20
MIL content (solvent evaporation at 210ºC)	10%	100	138	18
	20%	100	131	12
	40%	100	137	20

Table 1 reveals that the degree of crystallinity of the samples is significantly lower for the composite samples, indicating that the [Bmim][$FeCl_4$] acts as defect during the crystallization process. The addition of [Bmim][$FeCl_4$] changes the nucleation process inducing a growth in its kinetics, which leads to a defective crystallization of the P(VDF-TrFE) at the zones in contact to the MIL [27]. It is to notice that this effect is nearly independent of IL content or solvent evaporation temperature. The crystallization process around 90 ºC leads to slightly higher degrees of crystallinity, when compared to the other crystallization temperatures. This effect may be related to proximity of the ferroelectric-

paraelectric transition that occurs near this temperature, modifying the crystallization energetic landscape [27].

Figure 5 shows the TGA curves and the 1st derivate (DTG) curves of the P(VDF-TrFE)/[Bmim][$FeCl_4$] composite films. For all composites the weight loss is a multi-stage process.

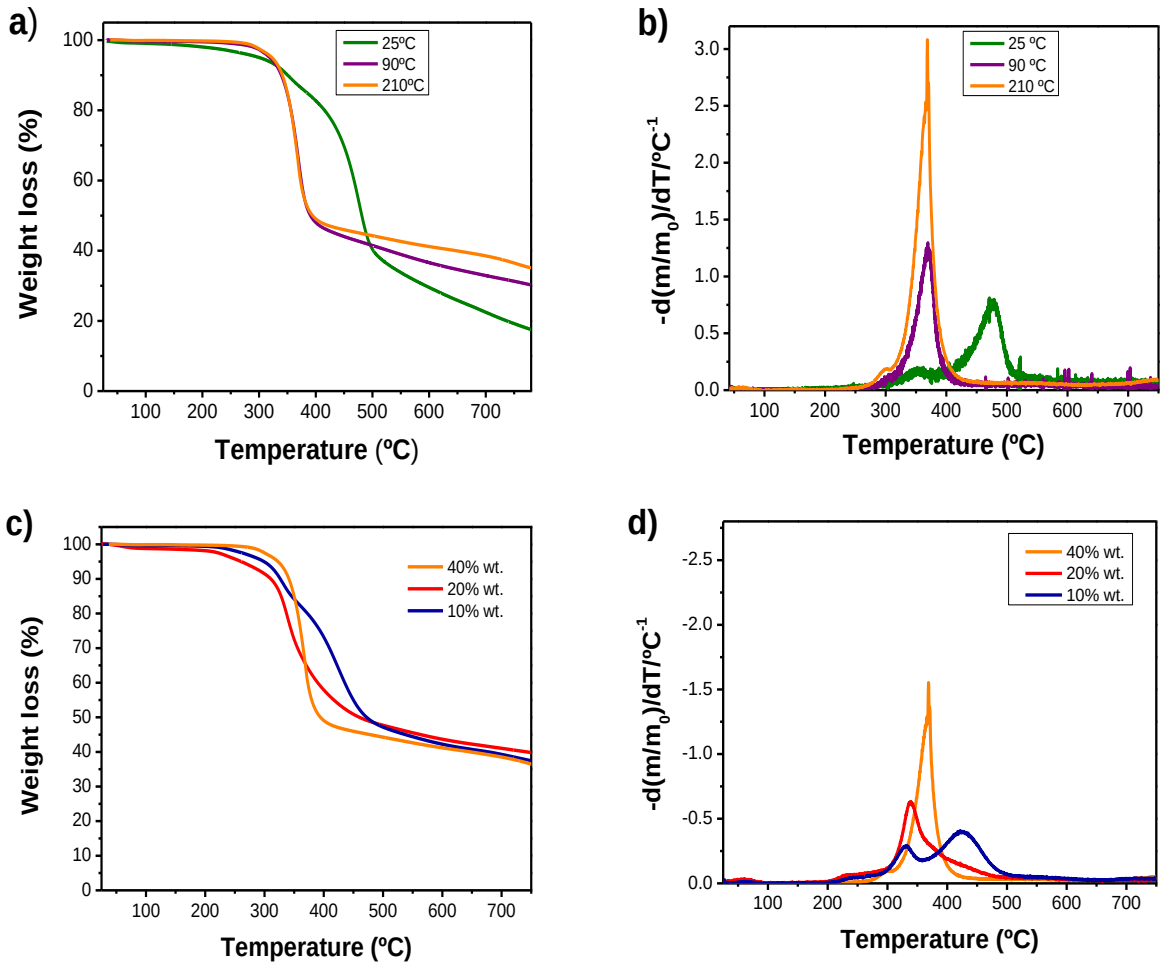

Figure 5. TGA (a,c) and DTG (b,d) curves of the P(VDF-TrFE)/[Bmim][$FeCl_4$] composites for: different solvent evaporation temperatures with 40% wt of MIL (a,b); for a solvent evaporation temperatures of 210 ºC and different IL contents (c,d).

A sharp weight loss with onset near 300 ºC is detected for the P(VDF-TrFE)/[Bmim][$FeCl_4$] composites containing 40% wt. of the MIL and for which the solvent was evaporated at 90 and 120 ºC (violet and orange lines in Figure 5a, respectively), and also for the composite sample dried at 210 ºC and incorporating 40% wt. of MIL (orange line in Figure 5c). This thermal event is attributed to the thermal degradation of [Bmim][$FeCl_4$], which is known to thermally decompose in a single step at ~330 ºC [24]. During the process the anions thermally decompose through dealkylation, whereas the cations mainly undergo alkyl migration and elimination reactions [28]. In the remaining samples the thermal decomposition starts at lower temperature. This effect is probably due to the progressive loss of occluded DMF (boiling temperature of 150 ºC). At temperatures higher than 400-450 ºC the degradation of P(VDF-TrFE) and the release of volatile compounds, such as hydrogen fluoride (HF), and small contents of 1,1,2-trifluoro-1,3-butadiene ($C_4H_3F_3$) and 1,2-difluoroethylene ($C_2H_2F_2$) [29], are responsible for the weight loss observed. At 750 ºC, about 30 % of the mass of practically all the samples remained to be thermally decomposed. The exception is the sample dried at room temperature and containing 40% wt. of MIL, for which the degradation process was more efficient (green line in Figure 5a).

Figure 5c shows that the highest onset temperature was observed at the highest MIL content.

3.5. Magnetic properties of the nanocomposites

Figure 6 presents the magnetic properties of the composites evaluated from VSM. The variation of magnetization with the applied magnetic field was also evaluated for [Bmim][$FeCl_4$].

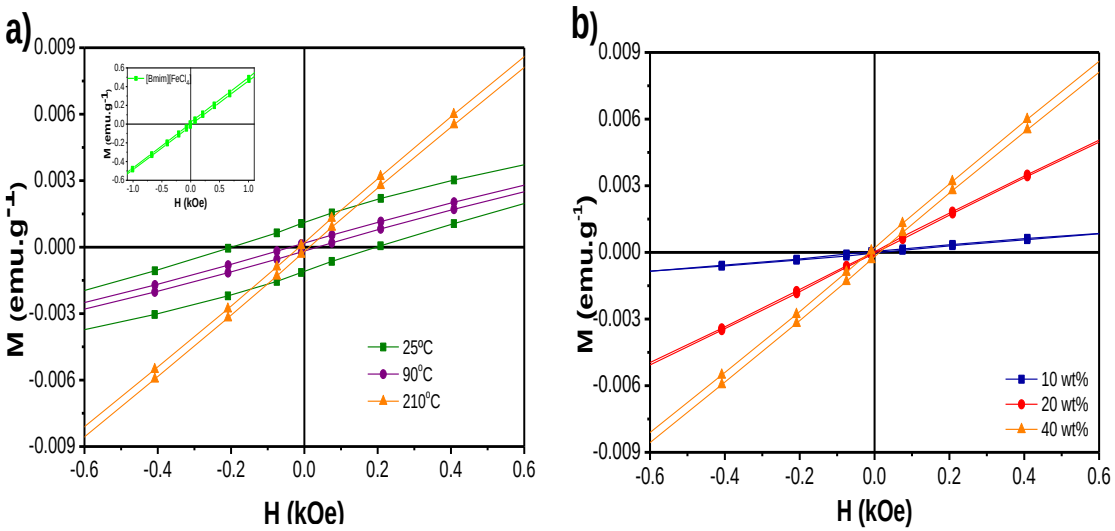

Figure 6. Magnetization of (a) P(VDF-TrFE)/[Bmim][$FeCl_4$] composites obtained at different temperatures for an IL content of 40% wt. Inset: pure IL [Bmim][$FeCl_4$]; and (b) for the composites with different IL contents as a function of applied magnetic field.

The inset of Figure 6a demonstrates that the IL exhibits a linear correlation with the applied magnetic field. This linear dependence on the magnetic field is also observed for the composites, both with varying IL content and solvent evaporation temperature. This behavior has already been reported for polymeric ILs and was related to the paramagnetic nature of the materials [30]. The magnetic susceptibility, related with the extent of magnetization of a material in response to a magnetic field, is similar for the samples prepared at room temperature or 90 ºC, but increases for samples prepared at 210 ºC, which can be related to the more compact structure and improved

entrapment/incorporation of the IL within the polymer structure. As expected, the magnetic susceptibility increase is proportional to the IL content, which allows to tune the magnetic response of the polymeric IL composites.

4. Conclusions

Magnetic P(VDF-TrFE)/[Bmim][$FeCl_4$] composites were synthesized at different solvent evaporation temperatures and at different [Bmim][$FeCl_4$] contents. The composites morphology is dependent on the evaporation temperature. No changes were detected in the chemical structure of the P(VDF-TrFE) polymer after incorporation of the MIL. The thermal characterization revealed a shift to lower temperatures of both the melting and Curie temperatures, indicating miscibility between the polymer and the MIL. Furthermore, the MIL incorporation led to a decrease in the degree of crystallinity (exceptionally for composites obtained at 90ºC) and at high MIL content to an increase of thermal stability, independent of the solvent evaporation temperature used during the composites preparation. Finally, an increase in the magnetic susceptibility was observed upon increasing IL content and solvent evaporation temperature.

ACKNOWLEDGMENTS

The authors thank FCT - Fundação para a Ciência e Tecnologia - for financial support under the framework of the Strategic Funding UID/FIS/04650/2013, and UID/QUI/50006/2013 and project PTDC/EEI-SII/5582/2014 by FEDER funds through the COMPETE 2020 – Programa Operacional Competitividade e Internacionalização (POCI) with the reference project POCI-01-0145-FEDER-006941. Funds provided by FCT in the framework of EuroNanoMed 2016 call, Project LungChek ENMed/0049/2016 are also gratefully acknowledged. FCT is also acknowledge by D.M.C. for the grants SFRH/BPD/96227/2013 and SFRH/BPD/121526/2016 and by J.M.S.S.E. for a contract (IF/00355/2012) under the Investigador FCT program. The authors acknowledge funding by the Spanish Ministry of Economy and Competitiveness (MINECO) through the project MAT2016-76039-C4-3-R (AEI/FEDER, UE) and from the Basque Government Industry Department under the ELKARTEK and HAZITEK programs. SGIker (UPV/EHU, MICINN, GV/EJ, ERDF and ESF) support is gratefully acknowledged.

5. References

1. Drossel, W. G.; Meinel, F.; Bucht, A.; Kunze, H., Smart materials for smart production – a cross-disciplinary innovation network in the field of smart materials. *Procedia Manufacturing* **2018,** *21*, 197-204.

2. Dias, J. C.; Martins, M. S.; Ribeiro, S.; Silva, M. M.; Esperanca, J.; Ribeiro, C.; Botelho, G.; Costa, C. M.; Lanceros-Mendez, S., Electromechanical actuators based on poly(vinylidene fluoride) with N-1 (1) (1) (2(OH)) NTf2 and C(2)mim C2SO4. *Journal of Materials Science* **2016,** *51* (20), 9490-9503.

3. (a) Nunes-Pereira, J.; Sencadas, V.; Correia, V.; Cardoso, V. F.; Han, W. H.; Rocha, J. G.; Lanceros-Mendez, S., Energy harvesting performance of BaTiO3/poly(vinylidene fluoride-trifluoroethylene) spin coated nanocomposites. *Composites Part B-Engineering* **2015,** *72*, 130-136; (b) Belhora, F.; Cottinet, P. J.; Hajjaji, A.; Guyomar, D.; Mazroui, M.; Lebrun, L.; Boughaleb, Y., Mechano-electrical conversion for harvesting energy with hybridization of electrostrictive polymers and electrets. *Sensors and Actuators a-Physical* **2013,** *201*, 58-65.

4. (a) Ribeiro, C.; Sencadas, V.; Correia, D. M.; Lanceros-Mendez, S., Piezoelectric polymers as biomaterials for tissue engineering applications. *Colloids and Surfaces B-Biointerfaces* **2015,** *136*, 46-55; (b) Pang, C.; Lee, C.; Suh, K. Y., Recent advances in flexible sensors for wearable and implantable devices. *Journal of Applied Polymer Science* **2013,** *130* (3), 1429-1441.

5. Teixeira, J.; Horta-Romaris, L.; Abad, M. J.; Costa, P.; Lanceros-Mendez, S., Piezoresistive response of extruded polyaniline/(styrene-butadiene-styrene) polymer blends for force and deformation sensors. *Materials & Design* **2018,** *141*, 1-8.

6. (a) Kim, K. J.; Tadokoro, S., *Electroactive Polymers for Robotic Applications: Artificial Muscles and Sensors*. Springer London: 2007; (b) Carpi, F.; Smela, E., *Biomedical Applications of Electroactive Polymer Actuators*. Wiley: 2009; (c) Bar-Cohen, Y., *Electroactive Polymer (EAP) Actuators as Artificial Muscles: Reality, Potential, and Challenges*. Society of Photo Optical: 2004; (d) Ribeiro, C.; Costa, C. M.; Correia, D. M.; Nunes-Pereira, J.; Oliveira, J.; Martins, P.; Goncalves, R.; Cardoso, V. F.; Lanceros-Mendez, S., Electroactive poly(vinylidene fluoride)-based structures for advanced applications. *Nature Protocols* **2018,** *13* (4), 681-704.

7. Cheng, Z. Y.; Zhang, Q. M., Field-activated electroactive polymers. *Mrs Bulletin* **2008,** *33* (3), 183-187.

8. Martins, P.; Lopes, A. C.; Lanceros-Mendez, S., Electroactive phases of poly(vinylidene fluoride): Determination, processing and applications. *Progress in Polymer Science* **2014,** *39* (4), 683-706.

9. Nunes-Pereira, J.; Sharma, P.; Fernandes, L. C.; Oliveira, J.; Moreira, J. A.; Sharma, R. K.; Lanceros-Mendez, S., Poly(vinylidene fluoride) composites with carbon nanotubes decorated with metal nanoparticles. *Composites Part B: Engineering* **2018,** *142*, 1-8.

10. Hayes, R.; Warr, G. G.; Atkin, R., Structure and Nanostructure in Ionic Liquids. *Chemical Reviews* **2015,** *115* (13), 6357-6426.

11. (a) Smiglak, M.; Reichert, W. M.; Holbrey, J. D.; Wilkes, J. S.; Sun, L.; Thrasher, J. S.; Kirichenko, K.; Singh, S.; Katritzky, A. R.; Rogers, R. D., Combustible ionic liquids by design: is laboratory safety another ionic liquid myth? *Chemical Communications* **2006,** (24), 2554-2556; (b) Costa, A. J. L.; Soromenho, M. R. C.; Shimizu, K.; Marrucho, I. M.; Esperanca, J.; Lopes, J. N. C.; Rebelo, L. P. N., Density, Thermal Expansion and Viscosity of Cholinium-Derived Ionic Liquids. *Chemphyschem* **2012,** *13* (7), 1902-1909.

12. Earle, M. J.; Esperança, J. M. S. S.; Gilea, M. A.; Canongia Lopes, J. N.; Rebelo, L. P. N.; Magee, J. W.; Seddon, K. R.; Widegren, J. A., The distillation and volatility of ionic liquids. *Nature* **2006,** *439*, 831.

13. (a) Zhang, S. G.; Zhang, Q. H.; Zhang, Y.; Chen, Z. J.; Watanabe, M.; Deng, Y. Q., Beyond solvents and electrolytes: Ionic liquids-based advanced functional materials. *Progress in Materials Science* **2016,** *77*, 80-124; (b) Correia, D. M.; Sabater i Serra, R.; Gómez Tejedor, J. A.; de Zea Bermudez, V.; Andrio Balado, A.; Meseguer-Dueñas, J. M.; Gomez Ribelles, J. L.; Lanceros-Méndez, S.; Costa, C. M., Ionic and conformational mobility in poly(vinylidene fluoride)/ionic liquid blends: Dielectric and electrical conductivity behavior. *Polymer* **2018,** *143*, 164-172.

14. Zai-Lai, X.; Andreas, T., Thermomorphic Behavior of the Ionic Liquids [C4mim][FeCl4] and [C12mim][FeCl4]. *ChemPhysChem* **2011,** *12* (2), 364-368.

15. (a) Joseph, A.; Żyła, G.; Ipe Thomas, V.; Radhakrishnan Nair, P.; Padmanabhan, A. S.; Mathew, S., *Paramagnetic Ionic Liquids for Advanced Applications: A Review*. 2016; Vol. 218, p 319-331; (b) Santos, E.; Albo, J.; Irabien, A., Magnetic ionic liquids: synthesis, properties and applications. *RSC Advances* **2014,** *4* (75), 40008-40018; (c) Cruz, M. M.; Borges, R. P.; Godinho, M.; Marques, C. S.; Langa, E.; Ribeiro, A. P. C.; Lourenço, M. J. V.; Santos, F. J. V.; Nieto de Castro, C. A.; Macatrão, M.; Tariq, M.; Esperança, J. M. S. S.; Canongia Lopes, J. N.; Afonso, C. A. M.; Rebelo, L. P. N., Thermophysical and magnetic studies of two paramagnetic liquid salts: [C4mim][FeCl4] and [P66614][FeCl4]. *Fluid Phase Equilibria* **2013,** *350*, 43-50.

16. Mejri, R.; Dias, J. C.; Hentati, S. B.; Martins, M. S.; Costa, C. M.; Lanceros-Mendez, S., Effect of anion type in the performance of ionic liquid/poly(vinylidene fluoride) electromechanical actuators. *Journal of Non-Crystalline Solids* **2016,** *453*, 8-15.

17. Smiglak, M.; Pringle, J. M.; Lu, X.; Han, L.; Zhang, S.; Gao, H.; MacFarlane, D. R.; Rogers, R. D., Ionic liquids for energy, materials, and medicine. *Chemical Communications* **2014,** *50* (66), 9228-9250.

18. Correia, D. M.; Martins, P.; Tariq, M.; Esperança, J. M. S. S.; Lanceros-Méndez, S., Low-field giant magneto-ionic response in polymer-based nanocomposites. *Nanoscale* **2018,** *10* (33), 15747-15754.

19. Nunes-Pereira, J.; Costa, C. M.; Leones, R.; Silva, M. M.; Lanceros-Mendez, S., Li-ion battery separator membranes based on poly(vinylidene fluoride-trifluoroethylene)/carbon nanotube composites. *Solid State Ionics* **2013,** *249*, 63-71.

20. Nunes-Pereira, J.; Ribeiro, S.; Ribeiro, C.; Gombek, C. J.; Gama, F. M.; Gomes, A. C.; Patterson, D. A.; Lanceros-Méndez, S., Poly(vinylidene fluoride) and copolymers as porous membranes for tissue engineering applications. *Polymer Testing* **2015,** *44*, 234-241.

21. Gonçalves, R.; Cardoso, V. F.; Pereira, N.; Oliveira, J.; Nunes-Pereira, J.; Costa, C. M.; Lanceros-Méndez, S., Evaluation of the Physicochemical Properties and Active Response of Piezoelectric Poly(vinylidene fluoride-co-trifluoroethylene) as a Function of Its Microstructure. *The Journal of Physical Chemistry C* **2018,** *122* (21), 11433-11441.

22. Faria, L. O.; Moreira, R. L., Infrared spectroscopic investigation of chain conformations and interactions in P(VDF-TrFE)/PMMA blends. *Journal of Polymer Science Part B-Polymer Physics* **2000,** *38* (1), 34-40.

23. Ferreira, J. C. C.; Monteiro, T. S.; Lopes, A. C.; Costa, C. M.; Silva, M. M.; Machado, A. V.; Lanceros-Mendez, S., Variation of the physicochemical and morphological characteristics of solvent casted poly(vinylidene fluoride) along its binary phase diagram with dimethylformamide. *Journal of Non-Crystalline Solids* **2015,** *412*, 16-23.

24. Xie, Z.-L.; Jelicic, A.; Wang, F.-P.; Rabu, P.; Friedrich, A.; Beuermann, S.; Taubert, A., Transparent, flexible, and paramagnetic ionogels based on PMMA and the iron-based ionic liquid 1-butyl-3-methylimidazolium tetrachloroferrate(III) Bmim FeCl4. *Journal of Materials Chemistry* **2010,** *20* (42), 9543-9549.

25. Leones, R.; Costa, C. M.; Machado, A. V.; Esperança, J. M. S. S.; Silva, M. M.; Lanceros-Méndez, S., Effect of Ionic Liquid Anion Type in the Performance of Solid Polymer Electrolytes Based on Poly(Vinylidene fluoride-trifluoroethylene). *Electroanalysis* **2015,** *27* (2), 457-464.

26. Nunes-Pereira, J.; Martins, P.; Cardoso, V. F.; Costa, C. M.; Lanceros-Méndez, S., A green solvent strategy for the development of piezoelectric poly(vinylidene fluoride–trifluoroethylene) films for sensors and actuators applications. *Materials & Design* **2016,** *104*, 183-189.

27. (a) Costa, C. M.; California, A.; Cardoso, V. F.; Sencadas, V.; Rodrigues, L. C.; Silva, M. M.; Lanceros-Méndez, S., Electroactive Poly(Vinylidene Fluoride-Trifluorethylene) (PVDF-TrFE) Microporous Membranes for Lithium-Ion Battery Applications. *Ferroelectrics* **2012,** *430* (1), 103-107; (b) Legrand, J. F., Structure and

ferroelectric properties of P(VDF-TrFE) copolymers. *Ferroelectrics* **1989,** *91* (1), 303-317.

28. Zhou, C.; Yu, X.; Ma, H.; Huang, X.; Zhang, H.; Jin, J., Properties and catalytic activity of magnetic and acidic ionic liquids: Experimental and molecular simulation. *Carbohydrate Polymers* **2014,** *105*, 300-307.

29. Correia, D. M.; Costa, C. M.; Nunes-Pereira, J.; Silva, M. M.; Botelho, G.; Ribelles, J. L. G.; Lanceros-Mendez, S., Physicochemical properties of poly(vinylidene fluoride-trifluoroethylene)/poly(ethylene oxide) blend membranes for lithium ion battery applications: Influence of poly(ethylene oxide) molecular weight. *Solid State Ionics* **2014,** *268*, 54-67.

30. Döbbelin, M.; Jovanovski, V.; Llarena, I.; Claros Marfil, L. J.; Cabañero, G.; Rodriguez, J.; Mecerreyes, D., Synthesis of paramagnetic polymers using ionic liquid chemistry. *Polymer Chemistry* **2011,** *2* (6), 1275-1278.

Table of Contents